BIOCHEMICAL PHARMACOLOGY 71 (2006) 1299–1307

available at www.sciencedirect.com

SCIENCE DIRECT®

journal homepage: www.elsevier.com/locate/biochempharm

The voltage dependence of recovery from use-dependent block by QX-222 separates mechanisms for drug egress in the cardiac sodium channel

Harvey A. Lardin, Peter J. Lee *

Section of Cardiology, Department of Medicine and Center for Cardiovascular Research, The University of Illinois at Chicago, Chicago, IL 60612, United States

ARTICLE INFO

Article history:
Received 21 December 2005
Accepted 18 January 2006

Keywords:
Voltage-gated sodium channel
Local anesthetic drug
QX-222
Use-dependent block
Voltage dependence of recovery
Isoform-specific residues

ABSTRACT

In neuronal sodium channels of squid giant axons, recovery from QX-222 block is slowed by hyperpolarization. However, in ventricular cells, hyperpolarization speeds recovery. Previously, we showed that isoform-specific residues in the external side of the cardiac sodium channel isoform (D1P-loop C373 and D4S6 T1752) influence use-dependent block (UDB) by lidocaine. To determine whether these isoformspecific residues contribute to the contrasting voltage-dependent recovery observed in ventricular myocytes, we measured recovery rates from UDB by QX-222 at holding potentials of 120, 140, 160 and 180 mV for wild-type cardiac channel (WT), the mutants C373Y (CY) and T1752V (TV), and C373Y/T1752V (CY/TV). Unlike neuronal channels, cardiac sodium channels recovered from QX block faster at hyperpolarized potentials. All mutations slowed QX-222 recovery, with the greatest rate reduction observed for the double mutant, indicating that the isoform-specific residues define external drug paths. The recovery rates varied linearly with voltage over the range tested, and we used the slopes of rate versus voltage plots to quantify voltage dependence. The TV mutation caused reduction in recovery rates without changing the slope, indicating that the mutation closed a voltage-independent egress path. The CY mutation, however, flattened the slope and reduced the voltage dependence of recovery. In addition, the reduction in rate caused by CY/TV is less than the sum of those for CY and TV, suggesting that the impacts of these two residues are interrelated. Therefore, we propose that the isoform-specific residues C373 and T1752 change recovery from UDB by distinct mechanisms but determine a common drug egress path.

1. Introduction

Class I local anesthetic antiarrhythmic drugs, reviewed in [1,2], block Na^+ current by binding to voltage-gated Na^+ channels. Local anesthetic drugs in clinical use are tertiary amines that exhibit both tonic and use-dependent block (UDB) of Na^+ current [3]. UDB by local anesthetic drugs is the hallmark of their antiarrhythmic activity because it enables them to be more effective when the frequency of action potentials is high, such as in ventricular tachycardia.

The UDB kinetics of these drugs can be explained by a combination of the modulated-receptor hypothesis [4,5]

* *Corresponding author at*: Section of Cardiology, Department of Medicine and Center for Cardiovascular Research, 840 S. Wood St. M/C 715, Chicago, IL 60612, United States. Tel.: +1 312 413 8573; fax: +1 312 996 5062.
E-mail address: peterl@uic.edu (P.J. Lee).
0006-2952/$ – see front matter
doi:10.1016/j.bcp.2006.01.010

and the guarded-receptor model [6,7], and are influenced by drug affinities toward different channel states, frequency and duration of action potentials, and drug access and egress paths. Using frog nerve, Courtney found that neuronal Na^+ channels recover from UDB by local anesthetic drugs in a voltage-dependent fashion, with the fastest rates of recovery occurring at depolarized potentials close to the threshold for activation [8]. Yeh and Tanguy [9] reported similar findings with the quaternary amine analogs of lidocaine, QX-222 and QX-314, in squid giant axons. They suggested that activation gate trapping of the charged drugs in the hydrophilic interior of the channel pore would bring about the observed behavior since the probability for channel gating (and the subsequent release of trapped drug) diminishes with increasing hyperpolarization. In contrast to what is seen with neuronal preparations, sodium currents in primary cardiocytes show the reverse trend in voltage-dependent recovery from block and recover faster upon hyperpolarization. Evidence of this behavior can be seen in early work by Weidmann [10] and was observed and characterized by Chen et al., as measured by V_{max} [11]. Subsequently, Hondeghem and Katzung [4], and Gintant and Hoffman [12] explained that this behavior is in keeping with the modulated-receptor hypothesis [5]. They suggested that recovery during hyperpolarization is facilitated by accelerating charged local anesthetic drugs along the membrane's electrical gradient. In the absence of trapping by the activation gate, as was seen by Yeh and Tanguy in neuronal channels, bound local anesthetic drug would dissociate more readily at hyperpolarized potentials. Makielski and Hanck reported similar behavior (in abstract form) as measured by I_{Na} in primary cardiocytes [13].

Previously, we demonstrated that isoform-specific residues defined lidocaine egress paths in the cardiac sodium channel [14]. Our study showed that isoform-specific residues in the upper part of domain 4 S6 (D4S6) (Thr in heart, Val in brain, and Cys in skeletal muscle) and the domain 1 P-loop (D1P) (Cys in heart, Phe in brain and Tyr in skeletal muscle) attenuated recovery from lidocaine UDB when mutated either to neuronal or skeletal isoform residues. These residues are also determinants for isoform specific external drug paths for quaternary amine derivatives of lidocaine [15,16]. The specific aim of this current study is to investigate whether these isoform-specific residues, which defined the external egress path for local anesthetic drugs, contributed to the differences in voltage dependence of recovery seen in cardiac and neuronal channels. We used a quaternary amine derivative of lidocaine, QX-222, to determine the impact of these isoform-specific residues on UDB recovery.

Using cloned $Na_v1.5$ channels expressing isoform-specific residues, we found that both isoform-specific residues in D1P and D4S6 significantly influenced UDB and drug recovery. However, while the residue in D4S6 has no influence on the voltage dependence of recovery, the residue in D1P alters the voltage-dependence of drug recovery. We propose a model in which the isoform-specific residues influence drug recovery in distinctive manners.

2. Materials and methods

2.1. Clones, molecular biology, and expression of Na^+ channels

The hH1a α-subunit was a gift from Dr. H.A. Hartmann [17]. When compared to the hH1 clone [18], hH1a is different from hH1 at four amino acid positions, including a deletion of Q1077. These differences do not result in significant differences in channel properties [19] (Lee, unpublished results). For historical reasons, we used the amino acid numbering of hH1 in the current study. For example, T1752 of hH1 occurs at the 1751st position in hH1a, but the TV mutation is designated T1752V. In all experiments, β1 was co-expressed with the α-subunit. Human β1 cDNA was cloned and sequenced to confirm the amino acid sequence. Typically, in order to express both in transfection, two separate plasmids containing the α- and β-subunits are mixed and co-transfected. However, assuring adequate expression of the β1-subunit for each α-subunit being expressed is difficult, as there is no independent method of quantifying its expression. Thus, we constructed an expression vector, which utilizes the internal ribosome entry sequence (IRES) to produce bicistronic messages to ensure a 1:1 (α1:β1) mRNA ratio. In brief, the vector contains a CMV promoter that drives the production of bicistronic mRNA containing the β1 cDNA in the 5′-side of the IRES and the α cDNA in the 3′-side of the IRES. The vector also has a separate GFP expression cassette. In transient transfection, cells that take up the plasmid can be identified by fluorescence within 18 h. Cells with green fluorescence were patched between 24 and 48 h. Almost all cells (>95%) patched contained inward sodium current between 500 pA and 5.0 nA (an improvement from transfection with a mixture of multiple plasmids). The presence of sodium current indicates production of intact bicistronic mRNA, since a truncated version lacks the poly-A tail and is held in the nucleus. We believe that this is an improved approach for co-expressing a consistent amount of β1. The mutants C373Y, T1752V, and C373Y/T1752V [14] were prepared by oligonucleotide-directed mutagenesis with the Quick Change Mutagenesis Kit (Stratagene) and subcloned into IRES constructs containing the WT channel.

Bicistronic plasmid vectors containing genes for the human β1-subunit and an α-subunit corresponding to hH1a WT, the P-loop mutant C373Y (CY), the D4S6 mutant T1752V (TV), or to the double mutant C373Y/T1752V (CY/TV) were expressed in HEK 293 cells [20] by transient transfection using the SuperFect® chemical transfection reagent, which was purchased from Qiagen. During transfection, cells were incubated 2–3 h at 37 °C in transfection medium, which consisted of DMEM, 30 μL of SuperFect®, and 5 μg of plasmid DNA. After application, the transfection medium was washed off and replaced by growth medium. The cells were incubated at 37 °C for another 24–48 h prior to experiments. Cells harvested for experiments were checked for the presence of green fluorescent protein as an indicator for vector expression. Typically, approximately 5% of transfected cells showed green fluorescence after 24 h, and these cells were patched. Inward currents were observed in most instances.

2.2. Electrophysiological recording and data analysis

Single-electrode voltage-clamp experiments were performed on HEK 293 cells with the Axon Instruments Axopatch 200B amplifier in whole cell configuration. Data acquisition was performed at a sampling rate of 20 kHz and filtered at 10 kHz. Data recording and analysis were done with the pCLAMP9 (Axon Instruments) software suite. The experimental chamber was kept at 25 °C and filled with extracellular buffer solution, which contained (in mmol) the following: NaCl 140, KCl 5, $CaCl_2$ 2, $MgCl_2$ 1, and HEPES 10. The pH was adjusted to 7.4 with NaOH. Patch electrodes were purchased from Harvard Apparatus and had resistances ranging from 0.8 to 1.5 MΩ. Electrodes were filled with buffer solution containing (in mmol) the following: NaCl 35, CsF 105, $MgCl_2$ 1, HEPES 10, and EGTA 10. Buffer pH was adjusted to 7.2 with CsOH. QX-222, 100 μM unless specified, was applied internally via the electrode buffer solution. QX-222 is susceptible to photodecomposition. In order to minimize decomposition, pipette solutions containing the drug were made fresh before experiments or were kept in the dark at −20 °C after preparation and thawed immediately before use. Leak currents ≤ 200 pA were subtracted, but experiments with leak currents ≥ 5% of peak current were discarded. Capacitance transients were cancelled, and series resistance was compensated electronically.

Data from current–voltage (−90 to +55 mV) experiments were normalized and fit according to the Boltzmann equation

$$I(V) = \frac{G_{max}(V - V_{rev})}{1 + e^{(V_{1/2}-V)/s}} \quad (1)$$

where $I(V)$ is the experimental membrane current as a function of membrane voltage, V, G_{max} is the maximum membrane conductance, V_{rev} is the reversal potential for sodium, $V_{1/2}$ membrane voltage at half-maximal conductance, and s is the slope factor. Pulses were 10 ms long. Steady-state inactivation (SSI) data were normalized and fit to the Boltzmann equation to determine I_{max}, $V_{1/2}$, and s. Holding potentials were sustained for 1 s, and test pulses were 10 ms long.

UDB recovery experiments with intracellular QX-222 were started 8–10 min after attaining whole-cell configuration, when peak inward currents did not change appreciably with infrequent pulses (every 30–60 s) to −10 mV from the holding

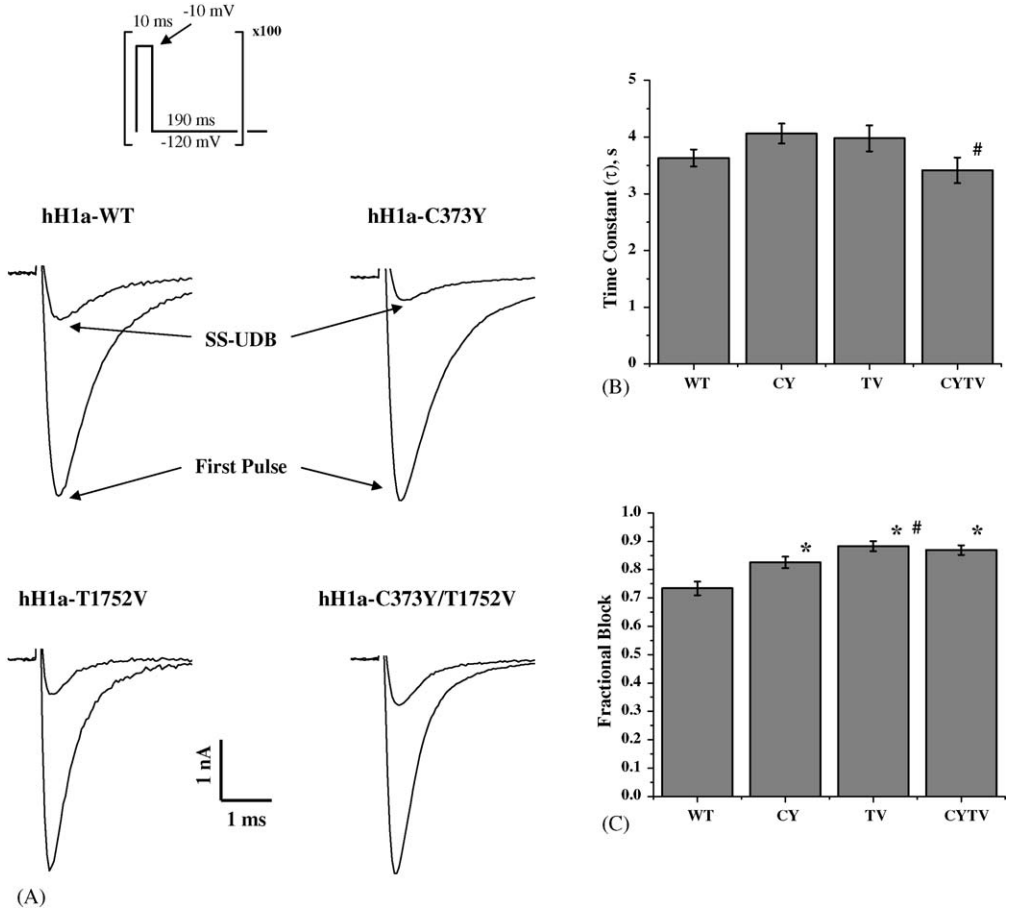

Fig. 1 – Use-dependent block (UDB) of WT hH1a sodium channel, the mutants C373Y and T1752V, and the double mutant C373Y/T1752V by 100 μM intracellular QX-222. All clones were expressed in HEK 293 cells by transient transfection. Inset: schematic of UDB pulse protocol (described in Section 2) showing UDB from holding potentials ranging from −120 to −180 mV. (A) Representative current tracings demonstrating the extent of UDB by QX-222 for each clone. The first pulse in the UDB train and a pulse representing steady-state block are shown. (B) Bar graph showing time constants (in units of s) for the onset of UDB (hundred 10 ms pulses at 5 Hz to −10 mV) by QX-222 for WT hH1a and mutants. (C) Bar graph showing steady-state fractional block resulting from UDB of WT hH1a and mutants. $^{*}p < 0.05$ vs. WT, $^{\#}p < 0.05$ vs. CY.

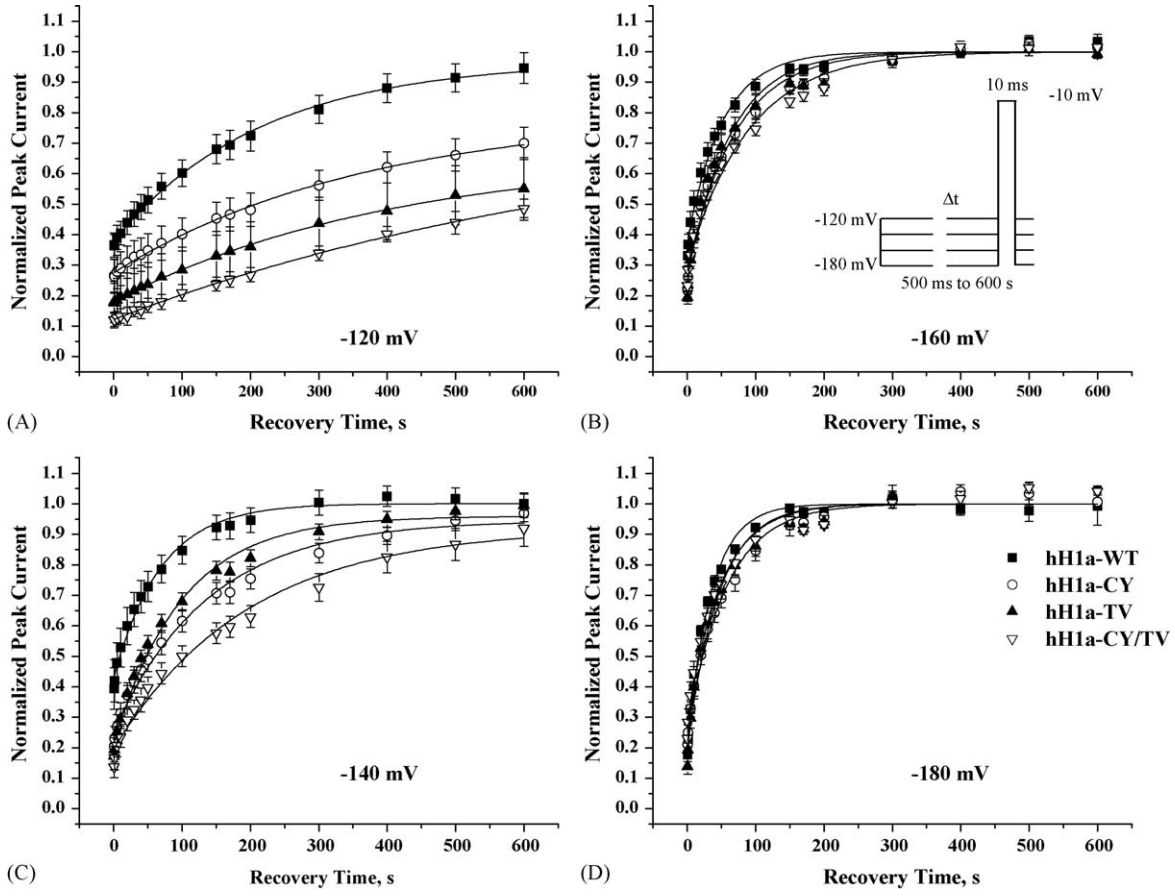

Fig. 2 – Plots of normalized peak current vs. UDB recovery time for WT hH1a sodium channel (solid squares), the mutants C373Y (open circles) and T1752V (solid triangles), and the double mutant C373Y/T1752V (inverted open triangles) at holding potentials of −120 mV (A), −140 mV (B), −160 mV (C), and −180 mV (D). Single-exponential decay best fits to the data sets are included for each clone at each holding potential. Inset: schematic representation of the pulse protocol used to measure recovery from UDB from 0.5 ms to 600 s after completion of the UDB protocol.

potential of −120 mV. For all UDB experiments, a single protocol was used, which consisted of a train of 100 successive 10 ms pulses from −120 to −10 mV at a frequency of 5 Hz (Fig. 1, inset). The development of UDB was fit according to a one-exponential function

$$I(t) = e^{-A(1/\tau)} + B \quad (2)$$

where I denotes the relative current as a function of cumulative time t, τ is the time constant of UDB onset, and B is the remaining current at the steady-state. $1 - B$, then, is the steady-state UDB level (ssUDB). Recovery from UDB at holding potentials of −120, −140, −160, and −180 mV was measured immediately after the UDB pulse train. All recovery protocols were identical, with the exception of the holding potential, and recovery times ranged from 500 ms to 600 s (Fig. 2, inset). Peak currents measured at each recovery pulse were normalized to a pre-UDB test pulse and fit according to a single-exponential decay function similar to Eq. (2). Data were analyzed with the Clampfit (Axon Instruments, CA) and Origin 7 (Originlab Corp., MA) software packages, and are reported as mean value ± S.E.M.

Recovery from channel inactivation in HEK 293 cells was assessed with a 1 s pre-pulse to −10 mV followed by a varying length of recovery time at a holding potential of −140 mV [21]. The data were fitted to a double-exponential equation to obtain time constants for fast and slow inactivation.

3. Results

3.1. QX-222 UDB of hH1a channels expressed in HEK 293 cells

In order to explore the voltage dependence of recovery, we used an HEK 293 mammalian expression system, in which a wider range of recovery voltages could be examined than previously reported in studies performed with primary cardiocytes or squid giant axons or with oocytes. Because we previously determined that the voltage dependence of recovery appeared to be related to the charged form of lidocaine [14], (Lee, unpublished results), we used QX-222 to compare UDB recovery in WT, CY, TV, and CY/TV clones. All of the following data were generated from sodium channel clones expressed in HEK 293 cells.

Representative current tracings that illustrate the extent of UDB (hundred 10 ms pulses to −10 mV from a holding potential of −120 mV at 5 Hz, over a period of 20 s) for WT

Table 1 – Single-exponential fitting parameters for use-dependent block by QX-222

	hH1a-WT	hH1a-C373Y	hH1a-T1752V	hH1a-(C373Y/T1752V)
τ	3.6 ± 0.2	4.1 ± 0.2	4.0 ± 0.2	3.4 ± 0.2
$(1 - b_\infty)$	0.734 ± 0.024	0.825 ± 0.020*	0.883 ± 0.018*,#	0.869 ± 0.017*

Fitting procedures are outlined in Section 2. Units of τ are in s. n = 20–34 for all clones.
* $P < 0.05$ vs. WT.
# $P < 0.05$ vs. CY.

and each of the mutant sodium channels are shown in Fig. 1a. At 100 μM (intracellular) QX-222, UDB developed with time constants of 3–4 s (17–20 pulses) for all clones (Fig. 1B, $p > 0.05$ versus WT for CY, TV, and CY/TV). Interestingly, the steady-state UDB estimated by one-exponential fitting was higher for CY, TV, and CY/TV than for WT (Fig. 1c, Table 1, $p < 0.05$ versus WT). In our previous study [14], differences in the steady-state UDB with lidocaine between the WT and mutant channels were not apparent, probably because of the fast recovery kinetics of neutral lidocaine that dominated the overall UDB. Here, when block is limited to the charged species of drug, a clear difference of UDB was demonstrated.

3.2. *Recovery from use-dependent block*

Recovery from UDB by 100 μM QX-222 was recorded as described in Section 2, and the pulse protocol is shown as an inset in Fig. 2. Initially, we observed the peak current elicited by 10 ms test pulses to −10 mV at varying time intervals over a cumulative recovery period that ranged from 1 ms to 60 s. A two-exponential equation was used for fitting. The faster time constants were approximately 10 to 20 ms and were not different among the clones (not shown). However, the recovery was very slow and incomplete after 60 s. Subsequently, we modified our protocol so that the cumulative recovery time period ranged from 0.5 to 600 s, and we adopted a one-exponential fitting Eq. (2) function. The UDB recovery experiments are illustrated in Fig. 2a–d for holding potentials of −120, −140, −160, and −180 mV, respectively. The time constants for recovery are listed in Table 2. Overall, all clones recovered slowly from QX-222 UDB, with time constants ranging in the tens of seconds to more than a thousand seconds over our voltage range. For each clone, recovery was slowest at −120 mV and fastest at −180 mV. Recovery from block at −120 mV was so slow that only WT recovered to its initial pre-UDB current after 600 s of recovery (95 ± 5%), while 70 ± 5% of CY, 55 ± 10% of TV and 49 ± 3% of CY/TV currents recovered (n = 5–9, $p < 0.05$ for all the mutants compared to WT). For the CY, TV, and CY/TV clones, an extrapolation to full recovery allowed us to fit the recovery accurately. As shown in Fig. 2 and Table 2, the recovery accelerated as the membrane potential became more hyperpolarized. All clones recovered completely at −160 and −180 mV. Frequently, cells could not be sustained at −180 mV for the full duration of the recovery protocol (600 s). However, the recovery at this potential was fast ($\tau \approx$ 33.2–57.1 s), and all experiments using cells that lasted at least 5 min ($>5\tau$) while holding the voltage clamp were used for analysis.

In order to compare the recovery processes among clones quantitatively, we inferred that UDB recovery followed a dissociation process independent of drug concentration, such that the rates can be approximated by $1/\tau$. Over the voltage range of our study, the rates for UDB recovery appeared linear (Fig. 3). Thus, we used linear regression to describe the voltage-dependence of UDB recovery and to compare the clones empirically. The fitting parameters for the linear regression (Fig. 3) are listed in Table 3. Interestingly, the fitted slopes for the WT and TV channels were similar (-4.3×10^{-4} and -4.2×10^{-4} s^{-1}, respectively), whereas introducing the CY D1P-loop mutation (CY and CY/TV channels) resulted in flattened voltage dependence (slopes, -2.7×10^{-4} and -2.6×10^{-4} mV^{-1} s^{-1}, respectively). At −120 mV, CY channels recovered faster than TV channels (time constants, p = 0.04, rates p = 0.10); but at more hyperpolarized potentials, TV channels appeared to recover faster. The two lines cross, signifying the disparate voltage dependences of recovery in the two channels by the different slopes. The faster recovery of the CY clone at −120 mV also correlates with slightly lower fractional UDB, as compared to TV ($p < 0.05$) and CY/TV (p = n.s.) in both cases.

In order to validate the unique impact of the D1P-loop residue on the voltage dependence of recovery, we measured recovery from UDB (250 μM QX-222) in $Na_v1.4$ (skeletal muscle

Table 2 – Single-exponential time constants for time-dependent recovery of WT and mutants from use-dependent block by QX-222

Holding potential (mV)	hH1a-WT	hH1a-C373Y	hH1a-T1752V	hH1a-(C373Y/T1752V)
−120	226.6 ± 17.5	621.6 ± 77.7*	1011.7 ± 170.9*,#	1164.9 ± 131.2*
−140	71.6 ± 4.4	149.8 ± 12.5*	115.3 ± 19.0*	258.1 ± 37.2*,#,†
−160	45.8 ± 4.8	74.9 ± 7.6*	59.2 ± 5.1	87.4 ± 3.2*,†
−180	33.4 ± 0.8	60.2 ± 6.7*	39.0 ± 4.9#	49.0 ± 4.3*

Fitting procedures are outlined in Section 2. Units are in s. n = 6–11 for all clones at all holding potentials.
* $P < 0.05$ vs. WT.
# $P < 0.05$ vs. CY.
† $P < 0.05$ vs. TV.

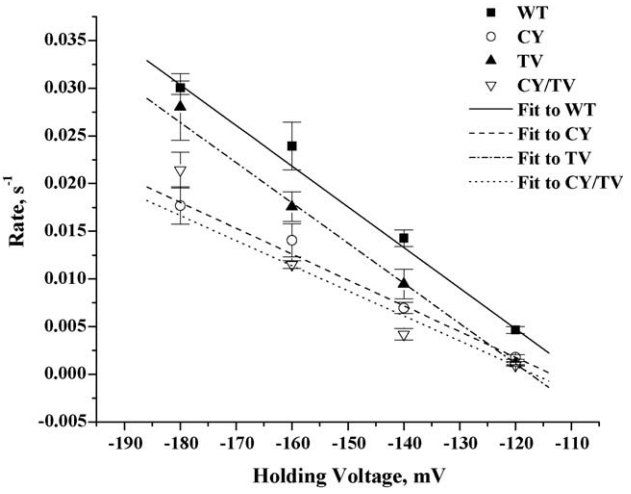

Fig. 3 – Plots of recovery rate vs. holding potential for WT hH1a sodium channel (solid squares), the mutants C373Y (open circles) and T1752V (solid triangles), and the double mutant C373Y/T1752V (inverted open triangles). Weighted linear best fit lines are included. Fitting parameters are listed in Table 3.

isoform μ1), where the equivalent residue for C373 in $Na_v1.5$ is Y401. Time constants were 331 ± 33 s at −120 mV ($n = 5$), 156 ± 33 s at −140 mV ($n = 5$), and 70 ± 9 s at −160 mV ($n = 6$). Linear regression analysis of the resulting recovery rates ($1/\tau$) versus holding potential resulted in a slope of $-2.8 \times 10^{-4}\ s^{-1}$, in good agreement with $Na_v1.5$ clones containing the CY mutation.

In summary, introduction of the isoform-specific mutations slowed UDB recovery significantly, suggesting that those residues define the external egress path for charged local anesthetic drugs, consistent with previous findings [14,22]. The voltage dependence of UDB recovery was qualitatively similar to what has been seen in native cardiac channels ($Na_v1.5$), and is the reverse of that seen in squid axons. In addition we found that the CY mutation altered the voltage dependence of UDB recovery significantly. The presence of the CY mutation (CY and CY/TV clones) resulted in attenuation of voltage-dependent drug egress, as manifested by reduction in the slopes of recovery rates. The TV mutation appeared to have no affect on voltage dependence while attenuating the recovery rates at a constant fixed level. Therefore, our data suggest that the two previously identified isoform-specific external residues have disparate influences on QX UDB recovery.

3.3. *Clones, activation, and inactivation of hH1a channels expressed in HEK 293 cells*

We tested the effects of the CY and TV mutations on basic channel properties (Table 4). Current-voltage relationships (IV) were not significantly altered with respect to WT, although all mutant channels show a slight trend toward activating at more depolarized potentials. Steady-state inactivation (SSI) shows a similar depolarizing shift in $V_{1/2}$ for all mutants with respect to WT, suggesting that the mutants also hinder the onset of inactivation. Recovery from inactivation was not altered and was fit best by a two-exponential equation. Fast time constants ranged from 4 to 7 ms, while slow time constants were under 100 ms, with the exception of the TV mutant ($p < 0.05$). Since we carried out our UDB and recovery experiments at hyperpolarized potentials ranging from −120 to −180 mV, and because QX-222 UDB recovery time constants ranged from tens of seconds to hundreds of seconds, mutation-dependent differences in QX UDB and recovery are not likely to be the result of differences in channel-gating properties. IV and SSI parameters for drug-bound channels are not included here because the kinetics of QX-222 recovery are too slow to be resolved by the standard IV and SSI pulse protocols. These SSI $V_{1/2}$ values are approximately 20 mV more negative than those reported previously for these clones [14]. This difference arises from the fact that the previous inactivation studies by Lee et al. were performed on channel clones expressed in oocytes rather than HEK 293 cells.

4. Discussion

In our study, we examined the importance of isoform-specific external residues in UDB and drug recovery in order to investigate the disparate behaviors in drug recovery of the sodium channel isoforms further. We found that cloned $Na_v1.5$ channels expressed in a heterologous system demonstrated similar drug-recovery kinetics as Purkinje fibers; i.e. hyperpolarization sped up drug recovery. Isoform-specific pharmacodynamics of antiarrhythmic drugs may have clinical implications since multiple isoforms of the voltage-gated Na^+ channels are found in the heart [23,24]. For example, neuronal channels are found in the T-tubules of cardiac myocytes and may modulate E–C coupling [25].

We initially postulated that mutations in the D1P-loop or D4S6 isoform-specific residues might greatly diminish, abolish, or even reverse the voltage dependence of recovery in the cardiac and neuronal isoforms. However, the isoform-specific mutations that ''closed'' the drug path [14,22] did not reverse

Table 3 – Parameters for linear regression analysis of unimolecular rates of recovery as a function of voltage

Clone	Slope, $mV^{-1}\ s^{-1}$	Intercept, s^{-1}	R^2
h-WT	$-4.3 \times 10^{-4} \pm 1.3 \times 10^{-5}$	−0.046 ± 0.002	0.998
h-C373Y	$-2.7 \times 10^{-4} \pm 2.1 \times 10^{-5}$	−0.031 ± 0.026	0.995
h-T1752V	$-4.2 \times 10^{-4} \pm 0.1 \times 10^{-5}$	−0.049 ± 0.001	1.000
h-(C373Y/T1752V)	$-2.6 \times 10^{-4} \pm 1.0 \times 10^{-5}$	−0.031 ± 0.001	0.977

Fits were weighted according to experimental uncertainties in rates.

Table 4 – Clones, activation, and inactivation

	hH1a-WT	hH1a-C373Y	hH1a-T1752V	hH1a-(C373Y/T1752V)
Inactivation				
a_F/τ_F	0.64 ± 0.04/6.5 ± 0.3	0.71 ± 0.03/4.3 ± 1.1	0.75 ± 0.02*/5.9 ± 1.0	0.75 ± 0.04/4.2 ± 1.0
a_S/τ_S	0.34 ± 0.04/95.5 ± 5.1	0.29 ± 0.02/73.7 ± 12.7	0.25 ± 0.02*/114.4 ± 21.7	0.24 ± 0.03/77.4 ± 9.3
IV				
$V_{1/2}$/slope (no drug)	−52.2 ± 2.9/5.4 ± 0.2	−47.0 ± 2.1/6.0# ± 0.2	−47.8 ± 1.4/5.8 ± 0.3	−47.8 ± 1.9/5.8 ± 0.3
SSI				
$V_{1/2}$/slope (no drug)	−95.6 ± 2.4/4.8 ± 0.2†	−87.2 ± 2.2*/4.6 ± 0.1†	−87.0 ± 2.1*/4.6 ± 0.1†	−89.06 ± 2.6/4.7 ± 0.2†

Fitting procedures are outlined in Section 2. In the upper half are two-exponential fit fast and slow amplitudes (a_F and a_S) and time constants (τ_F and τ_S) for recovery from fast and slow inactivation (n = 5–9 for all clones). Units of τ_F and τ_S are in ms. In the lower half, $V_{1/2}$ and Boltzmann slope parameters for steady-state inactivation (SSI) (n = 3–8 for all clones) and current–voltage relations (IV) (n = 3–9 for all clones) are listed. Units of $V_{1/2}$ are in mV.

* $P < 0.05$ vs. WT.

# $P < 0.05$ no drug vs. 100 μM QX-222 with IV data.

† $P < 0.05$ no drug vs. 100 μM QX-222 with SSI data.

or abolish the voltage dependence of UDB recovery of $Na_v1.5$. As was seen in the previous studies by Gintant & Hoffman [12] and Hanck and Makielski [13], we found that recovery of $Na_v1.5$ channels (the predominant cardiac isoform) sped up as the membrane was progressively hyperpolarized.

While both the CY and the TV mutations slowed the UDB recovery, we showed that the P-loop residue C373, unlike the D4S6 residue T1752, alters the voltage dependence of recovery from QX UDB. Although all clones recover faster from drug block with increasing hyperpolarization, the steepness of this voltage dependence is reduced by the presence of the CY mutation. The TV mutation, on the other hand, causes no change in voltage dependence and simply ''shifts'' the rate versus potential plot down. The individual contributions of the mutants to the voltage dependence of UDB recovery can be compared qualitatively. In going from WT to TV, the net effect of the TV mutation is to lower the rate of recovery by $-0.0038\ s^{-1}$ for all holding potentials, resulting in a voltage-independent reduction in the recovery. The effect of the CY mutation, however, is to flatten the slope of voltage dependence from −4.3 to $-2.7 \times 10^{-4}\ mV^{-1}\ s^{-1}$. The impact of the TV mutation in the CY channels also resulted in voltage-independent reduction of the recovery. The effect is more modest, with a uniform downward shift of $-0.0011\ s^{-1}$, less than a third of that observed in going from WT to TV. The effect of introducing the CY mutation to TV is seen in comparing TV and CY/TV. The net change, in this case, is similar to that seen when introducing the CY mutation to WT. The slope becomes shallower, and the resultant plot for CY/TV is parallel to that for CY. Therefore, the net contribution of introducing TV to any other clone is to cause a uniform reduction in recovery rate over the voltage range studied. This suggests that the TV mutation closes a voltage-independent external egress path available in WT and CY channels. The effects of introducing CY are voltage dependent, and appear to reduce the voltage dependence of UDB recovery for WT or TV to the same extent. It is also interesting to note that the addition of the CY mutation appears to cause a voltage-independent downward shift in addition to making the slope more shallow.

Do the distinct effects caused by the CY and TV mutations specify two distinct external egress pathways: one guarded by the D1P-loop residue C373 and the other guarded by the D4S6 residue T1752? Alternatively, do these residues contribute to a common external path in the hH1a channel? Previously, Qu et al. [26] found that the D4S6 residue T1755 (rH1) defined an external access path for QX314 that lies within the channel pore and that drug ingress and egress via this external pathway proceed through the channel pore. More recently, Sunami et al. [22] reported that the D1 P-loop residue C373 determined an external path for QX and found that the effects were roughly additive. Lee et al. [14] also found the effects of those two residues on the rate of recovery from lidocaine UDB to be roughly additive, suggesting that each residue might define a separate, independent drug path.

In the present study, we found that the effects of C373 and T1752 on drug recovery appear distinct but are not additive at every membrane holding potential. In Fig. 3, the change in voltage-dependence by introducing the CY mutation is the same for both CY and CY/TV channels. Likewise, introducing the TV mutation to WT (TV channels) or CY (CY/TV channels) slowed recovery to a constant degree. Both of these findings indicate distinct effects of these residues on drug recovery. However, over much of the voltage range, the rate reduction in the double mutant is significantly less than the sum of that caused by the single mutations. Adding the TV mutation to CY channels still results in voltage-independent reduction of recovery rates at all voltages, but to a lesser degree than the reduction seen when introducing the TV mutation to WT, as if the reduced voltage dependence caused by the CY mutation directly influenced the egress through the D4S6 path. Therefore, we will consider the possibility that D1P-loop and D4S6 residues may define a common egress path that is modulated in two distinct fashions.

We propose a simple qualitative model (illustrated in Fig. 4) to explain the voltage-dependent and voltage-independent effects caused by the C373Y and T1752V mutations, respectively. Residue C373, which is adjacent to the domain 1 selectivity-filter residue D372, is likely to be situated in the conducting pore and may contribute to the membrane electric field that is focused through the channel pore. It is possible that mutating the cysteine to tyrosine, a more polar residue, would reduce the shielding of the channel's outer vestibule from the membrane electric field. The result of this may be a shallower voltage gradient for a bound, charged QX-222 molecule and slower drug egress down the voltage gradient

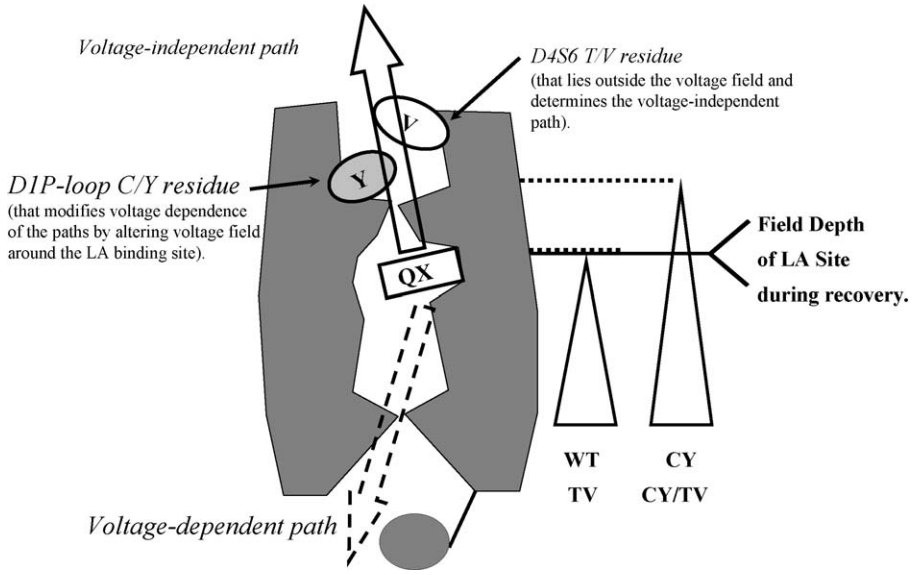

Fig. 4 – Schematic model of QX-222 recovery paths. QX-222, located at the local anesthetic binding site, may egress by an intracellular path (dashed arrow) or by an extracellular path (solid arrow). The residues Y373 and V1752 are indicated and correspond to the mutants C373Y and T1752V, respectively. At the right, the tapering triangles represent the effective membrane electric field strength as with respect to the charged drug's position within the channel pore.

toward the cytoplasmic side for CY channels, when compared to that in WT. This conclusion is supported by the shallower voltage-dependent recovery of QX-222 in Nav1.4 (Section 3). We propose a model in which the voltage-field is altered by the CY mutation so that the local anesthetic binding site now occupies a different voltage field depth in the closed channel. This model is qualitatively consistent with the results of Zamponi et al. [27]. Using a bilayer system, they found the electrical distance, $z\delta$, [3,28] for QX-314 bound to BTX-activated cardiac (Nav1.5) and skeletal sodium channels (Nav1.4) to be 0.33 and 0.24, respectively. The effects of the T1752 residue appeared to be voltage independent, indicating that the T1752 residue is largely outside the membrane electric field or that it lies in a shielded protein environment. When the P-loop residue C373 is mutated to Tyr, the T1752 egress path is also influenced in its voltage dependence. Perhaps the proximal part of the path is now within the electric field, and external drug egress is now influenced by hyperpolarization, resulting in a smaller impact of the TV mutation when the CY mutation is already present. This would also explain the apparent voltage-independent reduction in recovery rate that was observed by introducing the CY mutation to WT. If QX bound in the resting channel were to perceive an electric field that extends farther into the proximal part of the egress path defined by T1752, the voltage-independent rate of external egress defined by the D4S6 residue would decrease.

Our findings are consistent with a model in which QX-222 egresses from hH1a sodium channel via two distinct mechanisms: voltage-dependent and voltage-independent. The voltage-dependent mechanism can be attributed to cytoplasmic egress of the positively charged drug down the membrane electric field. As the membrane is progressively hyperpolarized, this egress mechanism dominates overall UDB recovery. The voltage-independent mechanism results from extracellular egress and is related to a path permitted by the presence of D4S6 residue T1752. We propose that the presence of the cardiac isoform-specific D1 P-loop residue C373 has an indirect effect, both on cytoplasmic egress and extracellular egress via the D4S6 pathway by changing the membrane electric field focused through the channel pore.

Acknowledgements

We would like to thank Drs. Harry Fozzard and Dorothy Hanck for helpful discussions. This study was supported by National Institutes of Health grants HL072742 (HAL) and HL72529 (PJL).

REFERENCES

[1] Butterworth JF, Strichartz GR. Molecular mechanisms of local anesthesia: a review. Anesthesiology 1990;72:711–34.
[2] Roden DM. Is there a need for new antiarrhythmic drugs? Arch Mal Coeur Vaiss 1996;89(1):13–8.
[3] Hille B. Classical mechanisms of block, ion channels of excitable membranes Sunderland, MA: Sinauer; 2001, p. 503–37.
[4] Hondeghem LM, Katzung BG. Time- and voltage-dependent interactions of antiarrhythmic drugs with cardiac sodium channels. Biochim Biophys Acta 1977;472:373–98.
[5] Hille B. Local anesthetics: hydrophilic and hydrophobic pathways for the drug-receptor reaction. J Gen Physiol 1977;69:497–515.
[6] Starmer CF, Grant AO, Strauss HC. Mechanisms of use-dependent block of sodium channels in excitable membranes by local anesthetics. Biophys J 1984;46:15–27.
[7] Starmer CF, Grant AO. Phasic ion channel blockade. A kinetic model and parameter estimation procedure. Mol Pharmacol 1985;28:348–56.
[8] Courtney KR. Mechanism of frequency-dependent inhibition of sodium currents in frog myelinated nerve by

the lidocaine derivative GEA. J Pharmacol Exp Ther 1975;195:225–36.
[9] Yeh JZ, Tanguy J. Na channel activation gate modulates slow recovery from use-dependent block by local anesthetics in squid giant axons. Biophys J 1985;47: 685–94.
[10] Weidmann S. Effects of calcium ions and local anesthetics on electrical properties of Purkinje fibres. J Physiol 1955;129:568–82.
[11] Chen CM, Gettes LS, Katzung BG. Effect of lidocaine and quinidine on steady-state characteristics and recovery kinetics of (dV/dt) max in guinea pig ventricular myocardium. Circ Res 1975;37:20–9.
[12] Gintant GA, Hoffman BF. Use-dependent block of cardiac sodium channels by quaternary derivatives of lidocaine. Pflugers Arch 1984;400:121–9.
[13] Hanck DA, Makielski JC. Hyperpolarization enhances use and rest recovery of QX-222 blocked cardiac sodium channels. Circulation 1989;80. II-605.
[14] Lee PJ, Sunami A, Fozzard HA. Cardiac-specific external paths for lidocaine, defined by isoform-specific residues, accelerate recovery from use-dependent block. Circ Res 2001;89:1014–21.
[15] Sunami A, Glaaser IW, Fozzard HA. Structural and gating changes of the sodium channel induced by mutation of a residue in the upper third of IVS6, creating an external access path for local anesthetics. Mol Pharmacol 2001;59:684–91.
[16] Qu Y, Rogers J, Tanada T, Scheuer T, Catterall WA. Molecular determinants of drug access to the receptor site for antiarrhythmic drugs in the cardiac Na^+ channel. Proc Natl Acad Sci USA 1995;92:11839–43.
[17] Hartmann HA, Tiedeman AA, Chen SF, Brown AM, Kirsch GE. Effects of III–IV linker mutations on human heart Na^+ channel inactivation gating. Circ Res 1994; 75:114–22.
[18] Gellens ME, George Jr AL, Chen LQ, Chahine M, Horn R, Barchi RL, et al. Primary structure and functional expression of the human cardiac tetrodotoxin-insensitive voltage-dependent sodium channel. Proc Natl Acad Sci USA 1992;89:554–8.
[19] Makielski JC, Ye B, Valdivia CR, Pagel MD, Pu J, Tester DJ, et al. A ubiquitous splice variant and a common polymorphism affect heterologous expression of recombinant human SCN5A heart sodium channels. Circ Res 2003;93:821–8.
[20] Graham FL, Smiley J, Russell WC, Nairn R. Characteristics of a human cell line transformed by DNA from human adenovirus type 5. J Gen Virol 1977;36:59–74.
[21] Kambouris NG, Hastings LA, Stepanovic S, Marban E, Tomaselli GF, Balser JR. Mechanistic link between lidocaine block and inactivation probed by outer pore mutations in the rat μ1 skeletal muscle sodium channel. J Physiol 1998;512:693–705.
[22] Sunami A, Glaaser IW, Fozzard HA. A critical residue for isoform difference in tetrodotoxin affinity is a molecular determinant of the external access path for local anesthetics in the cardiac sodium channel. Proc Natl Acad Sci USA 2000;97:2326–31.
[23] Dhar Malhotra J, Chen C, Rivolta I, Abriel H, Malhotra R, Mattei LN, et al. Characterization of sodium channel alpha- and beta-subunits in rat and mouse cardiac myocytes. Circulation 2001;103:1303–10.
[24] Maier SK, Westenbroek RE, McCormick KA, Curtis R, Scheuer T, Catterall WA. Distinct subcellular localization of different sodium channel alpha and beta subunits in single ventricular myocytes from mouse heart. Circulation 2004;109:1227–421.
[25] Maier SK, Westenbroek RE, Schenkman KA, Feigl EO, Scheuer T, Catterall WA. An unexpected role for brain-type sodium channels in coupling of cell surface depolarization to contraction in the heart. Proc Natl Acad Sci USA 2002;99:4073–8.
[26] Qu Y, Rogers J, Tanada T, Scheuer T, Catterall WA. Molecular determinants of drug access to the receptor site for antiarrhythmic drugs in the cardiac Na^+ channel. Proc Natl Acad Sci USA 1995;92:11839–43.
[27] Zamponi GW, Doyle DD, French RJ. Fast lidocaine block of cardiac and skeletal muscle sodium channels: one site with two routes of access. Biophys J 1993;65:80–90.
[28] Woodhull AM. Ionic blockage of sodium channels in nerve. J Gen Physiol 1973;61:687–708.